Detection of arsenic dopant atoms in a silicon crystal using a spherical aberration corrected scanning transmission electron microscope

Y. Oshima,* Y. Hashimoto, Y. Tanishiro, and K. Takayanagi
JST–CREST, 5-Sanbancho, Chiyoda-ku, Tokyo 102-0075, Japan
and Tokyo Institute of Technology, 2-12-1 Oh-okayama, Meguro-ku, Tokyo 152-8551, Japan

H. Sawada, T. Kaneyama, and Y. Kondo
JST–CREST, 5-Sanbancho, Chiyoda-ku, Tokyo 102-0075, Japan
and JEOL Ltd., 3-1-2 Musashino, Akishima, Tokyo 196-8558, Japan

N. Hashikawa and K. Asayama
Renesas Technology Corp., 5-20-1 Josuihon-cho, Kodaira, Tokyo 187-8588, Japan
(Received 29 September 2009; revised manuscript received 7 December 2009; published 11 January 2010)

In recent silicon transistors, fluctuation of the gate threshold voltage due to statistical variation in the number of dopant atoms has been pointed out to be a serious problem. For this reason, characterization methods are required which can detect individual dopant atoms within the transistor. In this paper, we present a technique for visualizing individual arsenic (As) atoms in a doped silicon crystal using our developed spherical aberration corrected scanning transmission electron microscope (STEM) with a convergent electron probe with a half angle of 30 mrad to view very thin doped silicon crystals from the [001] direction. The STEM images show the distribution of As dopant atoms within a 2.7 nm defocusing range around the focal position. It was found that in a highly doped silicon wafer following rapid thermal annealing, clustering of As atoms was extremely rare.

DOI: 10.1103/PhysRevB.81.035317 PACS number(s): 68.37.Ma, 61.72.S−, 61.72.uf

I. INTRODUCTION

With the downsizing of silicon-based transistors, statistical deviations in the number of dopant atoms can no longer be ignored. For a transistor with a 0.5 μm channel length, a deviation of about 2000 dopant atoms causes fluctuation in the gate threshold voltage.[1] Since transistors in commercial devices have channel lengths below 50 nm, not only statistical fluctuations in doping levels but also positional variation in the dopant atoms among the transistors has been pointed out to be a serious problem.[2–7] In device simulations, three-dimensional (3D) dopant distributions have been incorporated in order to investigate such characteristic fluctuations.[8] Experimentally, the gate threshold voltage has been demonstrated to be controllable by fabricating ordered dopant arrays in the channel region.[9] Scanning tunneling microscopy[10] and scanning spreading resistance microscopy experiments showed that the gate threshold voltage change depended on the cross-sectional mapping of the carrier concentration[11] but these studies lacked atomic-scale resolution, and the relationship between the carrier concentration and dopant distribution was not clarified. Furthermore, in high concentrations, the dopants have been reported to form electrically inactive clusters, which deteriorate the performance of the transistors. For these reasons, it is necessary to detect individual dopant atoms in transistors with atomic-scale precision.

High-angle annular dark-field scanning transmission electron microscopy (HAADF-STEM) is a very powerful method to obtain atomic resolution images, in which the intensity roughly correlates to the atomic number (Z) of atoms along each illuminated atomic column.[12] Muller's group has successfully observed antimony (Sb)-doped silicon along the [110] direction, and clearly distinguished the atomic columns with and without Sb atoms.[13,14] However, individual atoms of common dopant elements [arsenic (As), phosphorus (P), and boron (B)] in a silicon crystal have not yet been clearly imaged,[15] although arsenic Cottrell atmospheres around silicon defects[16] and arsenic atoms at a silicon grain boundary[17] have been observed.

Recently, spherical aberration corrected electron microscopes have been developed to yield scientific insights at an atomic scale since sharp electron probes with large convergent angles can be realized.[18–22] In simulation, such probes allow not only improved transverse resolution but also depth resolution on a nanometer scale.[23] Thereby, the contrast is expected to be enhanced for elements around the focal position. For crystalline materials, the channeling effect, which degrades the depth resolution, has been reported to be suppressible by reducing the energy spread of electrons.[24] Our developed spherical aberration corrected electron microscope (R005) (Ref. 22) (E=300 kV) has a half-convergent angle of 30 mrad, and a cold-field-emission gun with a small energy deviation ($\Delta E/E$=10^{-6}), allowing visualization of As atoms doped in a silicon crystal.

In this study, using our new microscope, a quasi-two-dimensional (2D) distribution of As atoms in a doped silicon crystal was observed from the [001] direction. This is because, by viewing along the [001] direction, strong 111 diffractions are never excited. In fact, it is difficult to take an atom-resolved STEM image along the [001] direction without the use of a spherical aberration corrector whereas this is relatively easy along the [110] direction. Therefore, in viewing along the [001] direction, the multiple-scattering (channeling) effect must be suppressed, suggesting that information around the focal position would be enhanced using the spherical aberration corrected electron microscope. In other

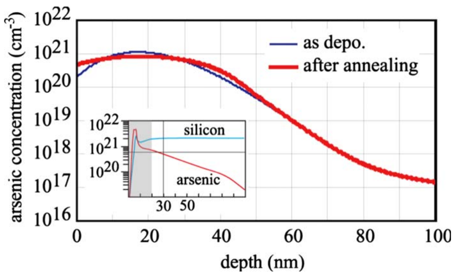

FIG. 1. (Color online) Simulation of distribution of arsenic (As) atoms in silicon crystal as a function of depth from the wafer surface. The As atoms are concentrated around 20 nm from the surface in the as-deposited sample (bold blue/dark gray curve) while it spreads to a depth of 10–30 nm from the surface after annealing (thick red/gray curve). Inset is the result of secondary-ion mass spectroscopy. The ordinate is the concentration, where the abscissa is the depth. Arsenic is red (gray) and silicon is blue (light gray). The thin horizontal line corresponds to 6.5×10^{20} cm^{-3} and the vertical line to 30 nm in depth.

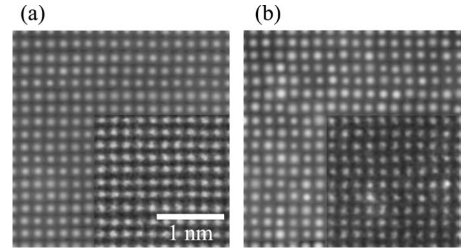

FIG. 2. (a) Typical processed STEM image of a nondoped area viewed from the [001] direction. Horizontal and vertical axes represent the [110] and $[1\bar{1}0]$ directions, respectively. All columns in the 16×16 array have a similar contrast. A raw STEM image is shown at the lower right (contrast is enhanced to distinguish the raw and processed images). (b) Typical processed STEM image of As-doped area viewed from the [001] direction. Some columns are clearly brighter than others. These columns contain one or more As atoms in a certain defocusing range around the focal position. A raw STEM image is shown at the lower right.

words, As atoms around the focal position would show stronger contrast.

II. EXPERIMENTAL

A silicon wafer was doped by As-ion implantation at 30 keV, and then annealed at 1300 K for just 10 s in order to produce an almost uniform distribution of As-doped atoms at a depth of 10–30 nm from the wafer surface as shown in Fig. 1. As seen in the inset of Fig. 1, the concentration of As dopant atoms was estimated to be 5.5×10^{20} cm^{-3} at a depth of around 30 nm and 6.5×10^{20} cm^{-3} at a depth of around 20 nm by secondary-ion mass spectroscopy (SIMS), which is typical of recent devices, although the concentration could not be measured correctly for regions above this due to instability of the ionization energy. The specimens for STEM observation were carefully thinned from the back side of the [001] wafer by mechanical polishing and dimpling, and further thinned by low-angle ion milling from both sides to remove amorphous layers. The specimens were obtained from about 10 nm below the original surface, although the precise depth is not known. Therefore, the concentration of As dopant atoms was estimated to be $6\pm0.5\times10^{20}$ cm^{-3} (1.2%). From among many specimens, we selected the thinnest one, which was estimated to be about 10 nm in thickness, based on electron energy-loss spectroscopy. During STEM observations, the probe current was 30 pA. The HAADF-STEM images were obtained by detecting electrons scattered from semiangles of 60–160 mrad. The exposure time per pixel in the STEM image was 38 μs. For a specimen thickness of approximately 10 nm, the number of electrons collected at the annular detector was in the range from 80 to 120.

In the quantitative analysis, the intensity of each column was obtained by fitting a 2D Gaussian function to the raw data. This was performed using the Levenberg-Marquardt algorithm, which is a standard method in nonlinear fitting.[25] The column intensity is defined as the amplitude of the fitted curve ignoring background roughness. No Fourier filtering was carried out, as pointed out in a previous report.[14] Regarding dopant analysis, Voyles *et al.*[14] proposed three quantitative criteria for whether or not a set of images shows contrast due to a single atom: (1) identification of the concentration, (2) explanation of the contrast, and (3) a null test, which means that there should be no pronounced intensity in the STEM image of pure crystalline silicon. In this study, we applied these criteria to the imaging of individual As dopant atoms.

III. RESULTS AND DISCUSSION

Figure 2(a) shows a typical processed HAADF-STEM image taken from a nondoped area (impurity concentration of less than 5×10^{10} cm^{-3}). The image in the inset is a raw STEM image, which shows prominent bright spots corresponding to atomic columns, all of which have a similar contrast. On the other hand, Fig. 2(b) shows a typical processed HAADF-STEM image taken from a doped area. It can be seen that some atomic columns exhibit prominently brighter contrast than others, and these brighter columns are distributed at random. The raw STEM image in the inset of Fig. 2(b) is confirmed to show similar brighter contrast. Such brighter columns were observed in about ten different doped areas but never in nondoped areas. It suggests that this bright contrast is not the result of either thickness variations or the presence of adsorbed molecules on the specimen surface but rather the existence of one or more As atoms in those columns.

For nondoped areas, the intensity histogram of approximately 3000 columns was reproduced by a Gaussian function with a standard deviation of 0.1 around the average intensity [Fig. 3(a)]. Taking into account that the intensity in the STEM image is proportional to the number of detected electrons, the latter is estimated to be approximately 100 because of the 10% statistical error. In fact, the number of electrons measured at the annular detector was in the range from 80 to 120. On the other hand, for the doped areas [Fig. 3(b)], the intensity histogram of approximately 3000 col-

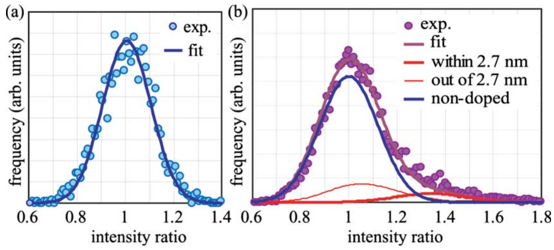

FIG. 3. (Color online) Histograms of column intensity ratios for nondoped and As-doped areas. (a) The ratio of the column intensity to the average intensity was obtained for approximately 3000 columns in several different nondoped areas. The vertical axis is the intensity ratio (the minimum unit is 0.01). The Gaussian function (blue/dark gray curve) has a standard deviation of 0.1 around the average intensity. (b) The column intensity normalized by the average intensity of the nondoped columns was obtained for approximately 3000 columns in several different As-doped areas. An enhanced tail appears in addition to the Gaussian distribution due to the nondoped columns. Fitting curve (bold purple/dark gray curve) is obtained for a 1.2% dopant concentration. It is composed of three different components: nondoped columns (bold blue/black curve), columns containing As atoms within the 2.7 nm range (bold red/gray curve), and containing As atoms outside of the 2.7 nm range (thin red/gray curve).

umns exhibits an enhanced tail at higher intensity superimposed on a Gaussian function similar to that for the nondoped areas. Therefore, the intensity component due to the doped columns, corresponding to the enhanced tail, broadens, which is different from the previous result for Sb-doped silicon, where the intensity was found to be constant regardless of the position of the Sb atom along the column.[13] Such broadening of the intensity histogram suggests that the image intensity of the column depends on the position of As atom along the column.

STEM images of a silicon (001) crystal doped with As atoms were simulated using multislice calculations.[26] The model structure consisted of 19 unit cells (10.3 nm thickness) along the [001] direction, where an As atom was substituted for a silicon atom located in the center of the column (the tenth cell from the top). As shown in Fig. 4, the intensity ratio of the doped to nondoped column was found to change depending on the focal position. A maximum ratio of 1.4 was obtained when the electron probe was focused on the doped atom, and a value of 1.3–1.4 was obtained within the 2.7 nm defocusing range while it decreased rapidly to 1.0 outside of this range. The simulation results suggest that the STEM image corresponds to a sectioning image of a 2.7-nm-thick slice around the focal position. When the substituting As atom was close to the top surface (the fourth cell from the top) or the bottom surface (the 16th cell from the top), the dependence of the intensity on the amount of defocus was similar to the case for an As atom in the middle of the column, and the defocusing range was calculated to be 3.3 and 2.7 nm, respectively. Although the defocusing range had a tendency to be slightly wider when the As atom was located near the top surface, this effect was small enough to be ignored.

We also calculated the intensities for double-doped columns on the condition that the first As atom substitutes for a

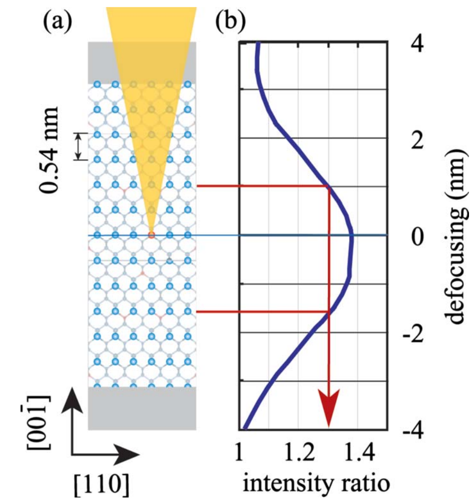

FIG. 4. (Color online) Simulated intensity ratio of an As-doped column to a nondoped one as a function of defocusing. (a) Schematic of the atomic arrangement on the [001] plane of As-doped silicon in which an As atom is located in the center. (b) Intensity ratio as a function of defocusing. The ordinate is the amount of defocus, where zero is defined as the position of the As atom. The abscissa is the intensity ratio. When focusing the probe within a 2.7 nm range around zero, the intensity ratio is above 1.3 (as indicated by the red arrow).

silicon atom located in the center of the column (the tenth cell from the top) and the focal position of the incident convergent electron beam is in the same plane as the As atom. The ratio of the intensity to that of the nondoped column is 1.40, 1.40, 1.52, 1.43, 1.41, and 1.40, respectively, when the second As atom substitutes for a silicon atom located at the first, third, fifth, 15th, 17th, and 19th cell from the top. The intensity ratio is not affected by placing the second As atom outside of the 5.4 nm defocusing range (corresponding to a thickness of ten unit cells). On the other hand, the intensity ratio is higher than 1.4 when the second As atom is located within the 5.4 nm defocusing range but its statistical probability is rare (below 0.05%) based on a binomial distribution.

Based on these results, we constructed theoretical intensity histograms for a 10-nm-thick silicon specimen with a concentration of As dopant of 1.0%, 1.2%, 1.4%, or 1.6%. The dopant atoms were assumed to be fairly uniformly distributed within the specimen. The ratios of nondoped, single-doped, and double-doped columns were determined using a binomial distribution and the defocusing dependence of the column intensity was based on the simulation results. Using the least-squares method, we found that the calculated histogram for the 1.2% concentration most closely matched the experimental results, as shown in Fig. 3(b). This is in accordance with the concentration estimated by SIMS. When the concentration was more than 1.4%, the area of the enhanced tail in the histogram became larger whereas when it was less than 1%, the area of the main peak became larger.

As shown in Fig. 3(b), the calculated histogram is composed of three different components: one representing nondoped columns, one representing columns containing one or two As atoms within the 2.7 nm defocusing range, and one

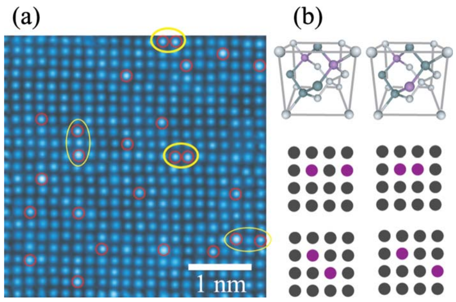

FIG. 5. (Color online) (a) Distribution of As atoms in the 2.7 nm defocusing range around the focal position. 25 columns (indicated by red/gray circles) have an intensity ratio of greater than 1.3. Most of these (probability of 70%) represent columns with As dopant atoms in the defocusing range. Thin and bold yellow/light gray ellipses indicate specific patterns of dopant clusters. (b) Model of dopant clusters. The left-side model is a donor pair, DP_2 (Ref. 27), showing two different patterns. One is two doped columns separated by twice the nearest-neighbor column distance and the other by the second-nearest-neighbor distance in the STEM image. The right-side model is a proposed structure referred to as a facing donor pair, FDP_2, showing two different patterns. One is two doped columns separated by the nearest-neighbor column distance and the other by the fourth nearest-neighbor distance.

representing all other doping cases. The two doping components have a Gaussian-type shape with center intensity ratios of 1.05 and 1.35 [indicated by thin and bold red/gray curves in Fig. 3(b), respectively]. The curves overlap to some extent, with an intersection point at roughly 1.3. About 70% of columns with an intensity ratio above 1.3 correspond to the case of a single or two As atoms within the 2.7 nm range.

In the HAADF-STEM image for the doped area shown in Fig. 5(a), the columns indicated by red circles have intensity ratios greater than 1.3 and represent 25 out of about 460 columns. Among these 25 columns, about 18 correspond to the case of a single or two As atoms within the 2.7 nm defocusing range. This result provides important information for investigating segregation of dopant atoms. Especially, it is possible to determine the types of dopant clusters that exist since the image is taken by viewing along the [001] direction. The left-side model of Fig. 5(b) is a dopant pair, DP_2.[27] The STEM image shows two different contrast patterns by viewing from the different [001] directions. One is two doped columns separated by twice the nearest-neighbor column distance and the other by the second-nearest neighbor. Therefore, in the [001] observation, these two patterns occur when a DP_2 cluster exists. Furthermore, we propose a new cluster named a "facing donor pair," FDP_2, as shown in the right side of Fig. 5(b) by taking into an account that a DP_2 is a kind of combination of two As atoms in a six-membered ring of silicon crystal. The facing donor pair has two As atoms facing each other in the six-membered ring. The STEM image shows two doped columns separated by the nearest-neighbor column distance and also by the fourth nearest-neighbor distance. In Fig. 5(a), two possible DP_2 clusters are indicated by thin yellow ellipses and two possible FDP_2 clusters by bold yellow ellipses, although the position of the dopant atoms on their respective columns cannot be precisely determined. In a total of ten different HAADF-STEM images, patterns such as those seen in Fig. 5(b) were observed only rarely. Although it is possible that such DP_2 or FDP_2 clusters exist in highly doped silicon following rapid thermal annealing, the probability of their occurrence seems very low.

We performed observations on As-doped silicon crystals with several specimen thicknesses and found that the increased brightness of the doped columns was more clearly visible for the thinnest specimens. We believe that this is due to the reduction in multiple-scattering effects in such thin specimens, leading to enhanced contrast within the defocusing range. The [001] observation results suggested the presence of certain types of dopant clusters, although the probability of their occurrence was very low. In the near future, we hope to obtain a 3D mapping of dopant atoms or clusters in silicon crystals by reducing the amount of statistical errors.

IV. CONCLUSION

Individual arsenic atoms in doped silicon crystal have been visualized using our developed spherical aberration corrected electron microscope (R005). By the use of a highly convergent electron probe and by viewing very thin doped silicon crystals along the [001] direction, arsenic dopant atoms were found to be uniformly distributed within a 2.7-nm-thick slice through the crystal. In the near future, it is expected that mapping of the three-dimensional dopant distribution in a silicon device will be possible.

*oshima.y.aa@m.titech.ac.jp

[1] T. Mizuno, J. Okumtura, and A. Toriumi, IEEE Trans. Electron Devices **41**, 2216 (1994).
[2] B. Hoeneisen and C. A. Mead, Solid-State Electron. **15**, 819 (1972).
[3] R. W. Keyes, IEEE J. Solid-State Circuits **10**, 245 (1975).
[4] H.-S. Wong and Y. Taur, Tech. Dig.-Int. Electron Devices Meet. **1993**, 705.
[5] M. R. Castell, D. A. Muller, and P. M. Voyles, Nature Mater. **2**, 129 (2003).
[6] S. Roy and A. Asenov, Science **309**, 388 (2005).
[7] See International Technology Roadmap for Semiconductor (ITRS) Report for supplementary online material, Update 2008. For more information on ITRS, see http://public.itrs.net/reports.html
[8] A. Asenov, Nanotechnology **10**, 153 (1999).
[9] T. Shinada, S. Okamoto, T. Kobayashi, and I. Ohdomari, Nature (London) **437**, 1128 (2005).
[10] H. Fukutome, Y. Momiyama, E. Yoshida, M. Okuno, and T. Itakura, Tech. Dig.-Int. Electron Devices Meet., **2005**, 897.

[11] L. Zhang, K. Ohuchi, K. Adachi, K. Ishimaru, M. Takayanagi, and A. Nishiyama, Appl. Phys. Lett. **90**, 192103 (2007).

[12] N. D. Browning, M. F. Chisholm, and S. J. Pennycook, Nature (London) **366**, 143 (1993).

[13] P. M. Voyles, D. A. Muller, J. L. Grazul, P. H. Citrin, and H. J. L. Gossmann, Nature (London) **416**, 826 (2002).

[14] P. M. Voyles, J. L. Grazul, and D. A. Muller, Ultramicroscopy **96**, 251 (2003).

[15] T. Yamazaki, K. Watanabe, Y. Kikuchi, M. Kawasaki, I. Hashimoto, and M. Shiojiri, Phys. Rev. B **61**, 13833 (2000).

[16] K. Thompson, P. L. Flaitz, P. Ronsheim, D. J. Larson, and T. F. Kelly, Science **317**, 1370 (2007).

[17] M. F. Chisholm, A. Maiti, S. J. Pennycook, and S. T. Pantelides, Phys. Rev. Lett. **81**, 132 (1998).

[18] M. Haider, S. Uhlemann, E. Schwan, H. Rose, B. Kabius, and K. Urban, Nature (London) **392**, 768 (1998).

[19] O. L. Krivanek, N. Dellby, and A. R. Lupini, Ultramicroscopy **78**, 1 (1999).

[20] C. L. Jia, M. Lentzen, and K. Urban, Science **299**, 870 (2003).

[21] S. J. Pennycook, M. Varela, C. J. D. Hetherington, and A. I. Kirkland, MRS Bull. **31**, 36 (2006).

[22] H. Sawada, F. Hosokawa, T. Kaneyama, T. Ishizawa, M. Terao, M. Kawazoe, T. Sannomiya, T. Tomita, Y. Kondo, T. Tanaka, Y. Oshima, Y. Tanishiro, N. Yamamoto, and K. Takayanagi, Jpn. J. Appl. Phys., Part 2 **46**, L568 (2007).

[23] E. C. Cosgriff and P. D. Nellist, Ultramicroscopy **107**, 626 (2007).

[24] A. Y. Borisevich, A. R. Lupini, S. Travaglini, and S. J. Pennycook, J. Electron Microsc. **55**, 7 (2006).

[25] D. W. Marquardt, SIAM J. Appl. Math. **11**, 431 (1963).

[26] K. Ishizuka, Ultramicroscopy **90**, 71 (2002).

[27] D. J. Chadi, P. H. Citrin, C. H. Park, D. L. Adler, M. A. Marcus, and H. J. Gossmann, Phys. Rev. Lett. **79**, 4834 (1997).